Biosensors and Bioelectronics 34 (2012) 137–143

Contents lists available at SciVerse ScienceDirect

Biosensors and Bioelectronics

journal homepage: www.elsevier.com/locate/bios

Preparation and application of novel nanocomposites of magnetic-Au nanorod in SPR biosensor

Hua Zhang[a], Ying Sun[a], Jing Wang[a], Jia Zhang[a], Hanqi Zhang[a], Hao Zhou[b], Daqian Song[a,*]

[a] College of Chemistry, Jilin University, Qianjin Street 2699, Changchun 130012, PR China
[b] Jilin Entry-Exit Inspection and Quarantine Bureau, Changchun 130062, PR China

ARTICLE INFO

Article history:
Received 14 November 2011
Received in revised form
31 December 2011
Accepted 26 January 2012
Available online 4 February 2012

Keywords:
Nanocomposite
Fe_3O_4–Au nanorod
Surface plasmon resonance (SPR)
Goat IgM

ABSTRACT

A novel nanocomposite Fe_3O_4–Au nanorod (AuNR) was prepared and used as the substrate in the surface plasmon resonance (SPR) biosensor to detect goat IgM. Fe_3O_4–AuNR nanocomposites were synthesized by a method of seed-mediated growth, and further characterized by molecular absorption spectroscopy, transmission electronic microscopy (TEM), energy-dispersive spectroscopy (EDS) and X-ray photoelectron spectroscopy (XPS). The nanocomposites exhibit both magnetic property and exceptional optical property, which are beneficial to the antibody immobilization and the sensitivity of detection. The sensing membrane can be regenerated easily and the experimental procedure is simplified. Moreover, the Au nanorods show two plasmon resonance wavelengths defined as transverse mode and longitudinal mode, and the longitudinal plasmon wavelengths are more sensitive to the changes in the dielectric properties of the surroundings. Fe_3O_4–AuNR nanocomposites got a high sensitivity in detection of antibody–antigen immunoassay. In the optimal conditions, the biosensor based on Fe_3O_4–AuNR nanocomposites exhibits a satisfactory response to goat IgM in the concentration range of 0.15–40.00 μg mL^{-1}. However, the biosensor without Fe_3O_4–AuNR nanocomposites shows a response to goat IgM in the concentration range of 1.25–40.00 μg mL^{-1}. As a result, the sensitivity of the biosensor based on Fe_3O_4–AuNR nanocomposites is enhanced significantly.

1. Introduction

Nanocomposites containing two or more different nanoscale functionalities can exhibit novel physical and chemical properties. There are two well-known composite systems including core/shell nanostructures (Peña et al., 2009; Malik et al., 2002) and exchange-coupled magnetic nanocomposites (Liu et al., 2002; Zeng et al., 2002), which have shown enhanced optical, magnetic and catalytic properties compared with their pure, single-component materials. Recently, combinations of magnetic nanoparticles and optical active components have drawn much attention, especially the combination of Au and magnetic nanoparticles. Core/shell Au@FePt nanoparticles (Härtling et al., 2010) and dumbbell-like Au–Fe_3O_4 nanoparticles (Yu et al., 2005) have been synthesized previously and showed interesting optical properties in Au and magnetic properties in FePt or Fe_3O_4. Magnetic nanoparticles as an immobilization matrix have increasingly been used in the area of bioscience during the past few years (Kouassi and Irudayaraj, 2006). Due to the unique magnetic features and high ratio of surface area to volume, magnetic nanoparticles also have been applied in bioseparation (Ito et al., 2005), DNA detection (Weizmann et al., 2003), drug delivery (Hu et al., 2008), and biosensors (Sun et al., 2007). However, pure magnetic particles are easy to aggregate and lack of activating group so that they are difficult to couple with biomolecules directly. Au is regarded as an excellent material in immunoassay owing to its prominent properties including exceptional optical property, water-solubility, good stability, significant biocompatibility and facility of surface functionality (Daniel and Astruc, 2004). In addition, the Au surface is quite suitable for thiol to bind stably. Au nanoparticles could be formed in various shapes involving nanospheres, nanocubes, nanobranches, nanorods and nanobipyramids, which showed different surface plasmon wavelengths to the refractive index of the surrounding medium (Chen et al., 2008). Spherical Au nanoparticles produce a strong absorption band around 520 nm, while Au nanorods exhibit two absorption bands: the transverse mode (520 nm) and the longitudinal mode (>600 nm, usually the end region of visible or near infrared region) (Eum et al., 2010). The longitudinal plasmon wavelengths are more sensitive to the changes in the dielectric properties of the surroundings and the sensitivity increases with the aspect ratio of the nanorods (Lee and El-Sayed, 2006; Jain et al., 2006; Link and El-Sayed, 2005). Therefore, Au nanorods are more sensitive for detecting biological molecules than nanoparticles with spherical structure. Recently researches on application

* Corresponding author. Tel.: +86 431 85168399; fax: +86 431 85168399.
E-mail address: songdq@jlu.edu.cn (D. Song).

0956-5663/$ – see front matter © 2012 Elsevier B.V. All rights reserved.
doi:10.1016/j.bios.2012.01.032

of Au nanorods to biosensing have become an increasing interest. Leong and co-workers have demonstrated the use of multifunctional Au nanorods for gene delivery (Salem et al., 2003). A new glucose biosensor based on the electron transfer and photothermal effect of Au nanorods was reported by Liu et al. (2010). The biosensor based on $Au_{rod}@SiO_2$ films was first used in colorimetric detection by Wang et al. (2006).

Surface plasmon resonance (SPR) biosensor has become an important tool for studying biomolecular interactions at a noble metal film surface, such as Au or Ag (He et al., 2004). The information of the biomolecular interactions can be obtained by measuring the optical characteristics (intensity, phase and polarization) of light reflected from the optical equipment (Law et al., 2011). For SPR biosensor provides many advantages such as real time, lable-free, and high sensitivity, it is widely applied for detecting the interactions between biomolecular partners, such as protein–protein (Fujino et al., 2003), protein–DNA (Hegde et al., 2004), drug–serum albumin (Rich et al., 2001), drug–liposome (Danelian et al., 2000) and especially antibody–antigen (Chou et al., 2004). In a traditional SPR system, the metal film substrate is usually coated with sulfhydryl compounds to form a sensing membrane, thus the receptor molecules such as antibody can be covalently immobilized on the activated surface (Wang et al., 2009). Effective immobilization of biomolecules on the surface of biosensor chip is crucial for the sensitivity enhancement of SPR biosensor and simplifying the immunoassay procedures.

IgM is a large (950 kDa) pentamer which contain five IgG-like monomers connected through a polypeptide chain rich in disulfide bonds and can be characterized by the presence of a disulfide-rich J chain (Caiazzo et al., 2009). Due to the pentameric structure, IgM antibodies are remarkable in immune response to most antigens and their presence in serum is a valuable indicator of running infections. Thus, it is of the essence to detect IgM in a rapid, accurate and sensitive way.

In this paper, a novel nanocomposite Fe_3O_4–Au nanorod (Fe_3O_4–AuNR) was prepared by a seed-mediated growth method (Pérez et al., 2007; Nikoobakht and El-Sayed, 2003) and applied in the SPR biosensor to amplify SPR response signal and simplify the immunoassay procedures. Compared with traditional biosensor immobilized with a self-assembled monolayer on the surface of Au film, Fe_3O_4–AuNR could be immobilized on the Au film with a magnetic pillar. The antibody was bound to Fe_3O_4–AuNR by MPA, and then the binding of antigen to antibody lead to change in the dielectric constant on the biosensor surface, which can be easily detected by the SPR biosensor.

2. Experimental

2.1. Materials

Goat IgM, rabbit anti-goat IgM and dog IgG were purchased from Beijing Boisynthesis Biotechnology Company. Bovine serum albumin (BSA) was purchased from Ding Guo Biotechnology Company (Beijing, China). 3-Mercaptopropinic acid (MPA), 1-ethyl-3-(3-dimethylaminopropyl)carbodiimide (EDC) and N-hydroxysuccinimide (NHS) were purchased from JK Chemical. Hydrogen tetrachloroauratehydrate ($HAuCl_4{\cdot}3H_2O$) was purchased from Acrosl. Ferric chloride hexahydrate ($FeCl_3{\cdot}6H_2O$), ferrous chloride tetrahydrate ($FeCl_2{\cdot}4H_2O$), sodium hydroxide, 3-aminopropyltrimethoxysilane (APTMS), silver nitrate, ethanol, cethltrimethlammonium bromide (CTAB), ascorbic acid and all other chemicals were of analytical reagent grade. All the solutions were prepared with ultra pure water, and all the glassware was cleaned with aqua regia before the experiments.

Goat IgM, rabbit anti-goat IgM and dog IgG were stored at −20 °C. Sodium phosphate buffered saline (PBS, 0.01 mol L^{-1}, pH 7.4) was used as running buffer.

2.2. Equipment

In this paper, the wavelength modulation SPR biosensor installed in our laboratory was used (Fig. S1). Kretschmann configuration was applied to achieve the resonant condition by attenuated total reflection (ATR) in a prism (Wang et al., 2011). A halogen tungsten lamp is used as the excitation light source. A 2 nm adhesive layer of Cr followed by 50 nm Au film was deposited on a K9 glass slide whose diameter and thickness were 12 and 0.7 mm, respectively. Then this glass slide was put on base of a prism (K9 glass) using a suitable index matching oil (cedar oil). A 100 μL flow cell was used for the reaction and magnetic pillar was immobilized under the optical prism. The diameter and height of the magnetic pillar are 25 and 12 mm, respectively. And the Au film was in the magnetic field of 750 G that was measured with Tesla meter. The light emitted from the lamp passes through the optical prism and excites surface plasmon at the interface between the Au film and the analytes. The output light is guided into the optical fiber and then enters the spectrophotometer (Ocean Optics, Inc., USA). A 2048 element linear array charge-coupled device (CCD) was used as the detector.

2.3. Assay procedure

2.3.1. Synthesis of Fe_3O_4 magnetic seeds

The Fe_3O_4 nanoparticles were used as seeds and prepared by chemical co-precipitation methods reported previously (Zhao et al., 2008). At first, $FeCl_3{\cdot}6H_2O$ (2.6 g), $FeCl_2{\cdot}4H_2O$ (1.0 g) and 12 mol L^{-1} HCl (0.425 mL) were dissolved in 15 mL deionized water to prepare a stock solution. Then the stock solution was added into NaOH solution (125 mL, 1.5 mol L^{-1}) drop by drop under nitrogen gas protection with the solution vigorously stirred at 80 °C. The obtained Fe_3O_4 nanoparticles were isolated from the solution with a permanent magnet and washed with deionized water four times. The nanoparticles were dispersed in 100 mL deionized water.

0.7 mL of Fe_3O_4 magnetic nanoparticle solution was dispersed into 50 mL ethanol by ultrasonic dispersion followed by dripping 0.4 mL of APTMS under stirring for 7 h at room temperature. The magnetic nanoparticles were isolated from the mixture with a permanent magnet and washed with ethanol and deionized water successively, then re-dispersed into 20 mL water and stored at 4 °C.

2.3.2. Preparation of Fe_3O_4–AuNR

The nanocomposites were produced by means of a seeded growth method (Pérez et al., 2007), in which the Fe_3O_4 nanoparticles were used as seeds. 3 mL of 0.05 (or 0.1) mmol L^{-1} $AgNO_3$ was added into 50.0 mL of 0.1 mol L^{-1} CTAB solution at 25 °C. 50.0 mL of 2 mmol L^{-1} $HAuCl_4$ was added into the solution to make up a growth solution. And 1.05 mL of 0.1 mol L^{-1} ascorbic acid was mixed with the growth solution, and the color changed from orange for Au^{3+}-CTAB complexes into colorless for Au^{+}-CTAB. Finally, 700 μL of magnetic seed solution was added. The temperature of the resulting solution was kept at 27–30 °C for 24 h to ensure the growth completely. The nanocomposites were precipitated with a permanent magnet. The supernatant solution was removed and the precipitate was re-dispersed in 30 mL deionized water. To characterize the nanocomposites, the molecular absorption spectroscopy, transmission electronic microscopy (TEM), energy-dispersive spectroscopy (EDS) and X-ray photoelectron spectroscopy (XPS) were applied.

2.3.3. Preparation of Fe_3O_4–AuNR/anti-goat IgM sensing membrane

The Fe_3O_4–AuNR nanocomposites solution was injected into the flow cell equipped with a magnetic pillar under the biosensor chip. Thus the nanocomposites can be immobilized on the biosensor chip through magneticaction, which resulted in a shift of the SPR resonant wavelength. After the immobilization was finished, 10 mmol L^{-1} MPA was injected into the flow cell and incubated for 6 h. Then the biosensor surface was activated with NHS (100 mg mL^{-1}) under the catalysis of EDC (100 mg mL^{-1}) for 20 min. PBS buffer was injected as the baseline solution. After the resonant wavelength kept constant, rabbit anti-goat IgM solutions were introduced into the flow cell to covalently attach to carboxyl-activated surfaces. After 12 h, PBS buffer was injected into the flow cell to wash off non-covalently bound antibody. In order to block the non-specific binding sites of activated carboxyl group, 1 mol L^{-1} ethanolamine hydrochloride solution (pH 8.0) was injected. 10 min later, PBS buffer was injected and the Fe_3O_4–AuNR/anti-goat IgM sensing membrane was formed. A schematic diagram of the experimental procedure is shown in Fig. 1.

For comparison, the MPA/anti-goat IgM sensing membrane without the nanocomposites was also constructed. PBS buffer was used as the baseline solution and 10 mmol L^{-1} MPA was injected into the flow cell. After 2 h, carboxyl group of MPA was activated with NHS under the catalysis of EDC for 20 min. 100 μg mL^{-1} rabbit anti-goat IgM solution was injected. The following processes were the same as those mentioned above.

2.3.4. Immunoassay

At room temperature, goat IgM at different concentrations was separately injected into the flow cell. The immunoreactions between goat IgM in the solution and the rabbit anti-goat IgM immobilized on the surface of biosensor chip leads to a shift of resonant wavelength that can be measured by SPR biosensor. Then PBS buffer was injected into the flow cell and another sample solution was injected.

To evaluate the selectivity of the method mentioned above, human IgG and BSA were determined by the same procedure.

2.3.5. Regeneration

The sensing membrane of the SPR biosensor was regenerated after a series of goat IgM immunoassays were performed. The magnetic pillar was taken away from the prism and water was injected into the flow cell to wash away the Fe_3O_4–AuNR nanocomposites coupled with anti-goat IgM. After 40 min, the conjugates could be removed from the Au film.

3. Results and discussions

3.1. Preparation and characterization of Fe_3O_4–AuNR nanocomposites

Fe_3O_4 nanoparticles were first synthesized by co-precipitation of aqueous Fe^{2+}/Fe^{3+} salt solutions under the basic condition. For the preparation of Fe_3O_4–AuNR nanocomposites, the popular seeded growth method (Nikoobakht and El-Sayed, 2003) was applied, with CTAB not only acting as a stabilizer for the colloids but also facilitating transport of Au ions and directing anisotropic growth. Specifically, the magnetic particles (Fe_3O_4) were used as seeds. Before the growth solution was added, the Fe_3O_4 nanoparticles were first modified with amino groups to provide heterogeneous nucleation positions for AuNR. The aspect ratio of AuNR can be controlled by adjusting the amount of seed solution, $AgNO_3$ solution, and ascorbic acid solution. Compared with the amount of seeds, the concentrations of Au and Ag ions have more significant effect on the size of the nanocomposites. It was reported that Au NRs made in the absence of Ag ions converted to Au nanospheres and the Ag ions restricted the growth and stabilized the NR surface (Jana et al., 2001). The reaction rate can be reduced in the presence of Ag ions, which is beneficial to obtain rod shapes. The reason may be that Ag ions can form a compact silver monolayer over the gold surface prior on the {1 1 0} facets to prevent further growth. The Ag monolayer can be oxidized and replaced by the gold ions from solution. The growth of gold on {1 1 0} facets slows down remarkably. {1 0 0} facets are only partially covered with silver and the rapid growth of the facets can result in one-dimensional growth along the {1 0 0} direction leading to nanorod formation (Pérez et al., 2007). The morphologies of Fe_3O_4 nanoparticles and Fe_3O_4–AuNR nanocomposites used in these experiments were characterized by TEM. As shown in Fig. 2a, the average size of Fe_3O_4 nanoparticles is about 10 nm and it can be seen that the nanoparticles are aggregative. Pure magnetic nanoparticles can form large aggregations, which is due to the high surface energy of the nanoparticles. On the other hand, there is magnetic attraction between Fe_3O_4 nanoparticles. Fig. 2b and c shows the TEM images corresponding to the two samples of nanocomposites obtained with 0.05 and 0.1 mmol L^{-1} $AgNO_3$, respectively. The mean particle sizes of the Fe_3O_4–AuNR are 50×15 nm and 65×30 nm, respectively. The AuNR grows only on one special spot of the Fe_3O_4 nanoparticles instead of covering the Fe_3O_4 nanoparticles completely and the core/shell structure cannot be formed. Because there is high interfacial energy between Au and magnetic nanoparticles, the Au prefers to start growing on the facet with the lowest interfacial energy. When Au is deposited on this facet of Fe_3O_4 nanoparticles, Au^+ ions remaining in the solution are easily reduced to Au^0 on the facet because of a self-catalyzed reduction of Au ions.

Energy dispersive spectroscopy was employed to determine the corresponding elements in the nanocomposites. It can be obviously seen from Fig. 2d that Fe and Au elements coexist in the nanocomposites. Because energy dispersive spectrometer was attached with a field emission scanning electron microscope (SEM), Al and Si elements occur in the energy dispersive spectrum. Furthermore, X-ray photoelectron spectroscopy was used to obtain key information concerning the chemical state of the nanocomposites. The binding energy for the C (1s) peak (284.7 eV) was used as an internal reference. Fig. 2e shows two intense peaks with the binding energies of 710.7 eV and 725.3 eV which are assigned to Fe ($2p_{3/2}$) and Fe ($2p_{1/2}$), respectively. The two peaks including Fe^{2+} (of FeO) and Fe^{3+} (of Fe_2O_3) peaks are typical characteristics of the Fe_3O_4 structure (Barr, 1978). The broad peak at 718.0 eV corresponds to Fe^{3+}. The Fe ($2p_{3/2}$) peak shifted slightly from 711.2 to 710.7 eV due to the addition of Au atoms, suggesting a strong electronic interaction between Au and Fe_3O_4 (Wang and Ro, 2006). Fig. 2f shows the X-ray photoelectron spectrum of Au (4f) of Fe_3O_4–AuNR nanocomposites. The peaks at 83.5 eV and 87.2 eV correspond to Au^0 $4f_{7/2}$ and Au^0 $4f_{5/2}$, respectively (Negishi et al., 2005). The results demonstrate the presence of Au atoms and Fe_3O_4 in the nanocomposites.

Fig. 3 shows UV–vis–NIR absorption spectra of Fe_3O_4 nanoparticles and Fe_3O_4–AuNR nanocomposites. It can be seen from Fig. 3A that the absorbance of Fe_3O_4 decreases and no obvious absorption peak is observed. When gold nanorods were introduced, Fe_3O_4–AuNR nanocomposites show two absorption peaks (Fig. 3B). When the concentration of $AgNO_3$ is 0.05 mmol L^{-1}, the absorption peaks located at around 567 nm and 967 nm arise from transverse and longitudinal resonances (Fig. 3a). When the concentration of $AgNO_3$ is 0.1 mmol L^{-1}, the transverse resonance peak is 563 nm, and the longitudinal resonance peak shifts to 1031 nm (Fig. 3b). Both the transverse plasmon wavelengths show a red shift compared with the adsorption wavelength of the single Au nanoparticles (520 nm), which is due to the loss of the electrons of Au surface. However, this spectrum is unexpected, which is

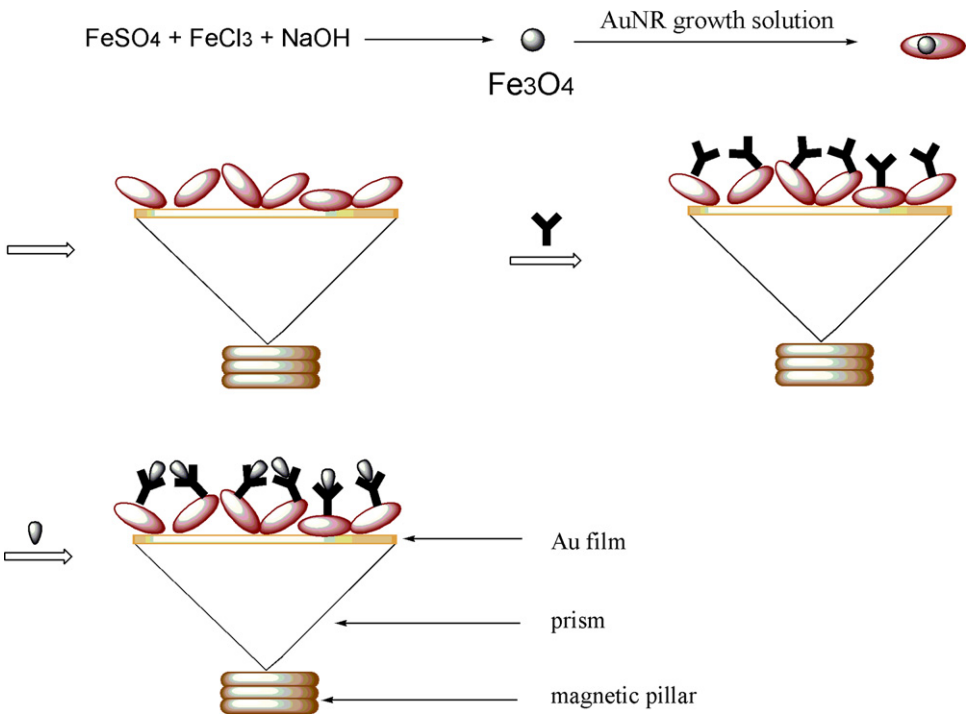

Fig. 1. A schematic diagram of the experimental procedure. ( ) Au nanorod, ( ) antibody, ( ) antigen.

dominant in the transverse plasmon resonance. It is possibly due to the presence of other shapes (mostly spheres) in the solution.

3.2. Preparation of SPR biosensor based on Fe_3O_4–AuNR

The Fe_3O_4–AuNR nanocomposites prepared with 0.05 mmol L^{-1} $AgNO_3$ were used in the following experiments. Different concentrations of Fe_3O_4–AuNR nanocomposites were injected into the flow cell to select the optimal condition. With a magnetic pillar under the prism, the modified magnetic nanocomposites can be immobilized on the Au film by magnetic force easily. Fig. S2 shows the immobilization process of the nanocomposites. The force exerted on the nanocomposites arises from the magnetic field and the gradient of the field. The shifts of the resonant wavelength resulted from the immobilization of the Fe_3O_4–AuNR nanocomposites were monitored in real time and got to a steady state in about 40 min (Fig. S3). The capture of the nanocomposites took such a long time because a high gradient of magnetic field did not occur at the sensor surface and the magnetic capture force was extremely weak. The result indicates that the resonant wavelength shifts increase gradually when the concentrations of the Fe_3O_4–AuNR nanocomposites increase from 0.10 g mL^{-1} to 0.50 g mL^{-1}. It is found out that the resonant wavelength reaches a level at the concentration higher than 0.40 g mL^{-1} and the maximum shift of the resonant wavelength is 2.89 nm.

The immobilization of nanocomposites was examined in the absence of magnetic pillar under the prism. There was nearly no change of the resonant wavelength in an hour, which indicated that the nanocomposites could hardly be immobilized without the magnetic binding force.

3.3. Immobilization of rabbit anti-goat IgM

After the surface of Au film was activated, rabbit anti-goat IgM at different concentrations was separately injected into the flow cell to select the optimal experiment conditions. The antibody can be immobilized on the Au film through covalent attachment between the amine group and the carboxyl group. Fig. 4a exhibits the kinetic adsorption curves of immobilizing rabbit anti-goat IgM at different concentrations. It is found that the resonant wavelength shifts distinctly at first and then changes slowly as time goes by. Finally, the resonant wavelength tends to be stable in 120 min, which indicates the immobilization of rabbit anti-goat IgM on the biosensor chip surface was completed. With the increase of the concentration of the rabbit anti-goat IgM, more and more antibodies were immobilized on the biosensor chip surface, which made the resonant wavelength move to longer wavelength. When the antibody immobilized on the surface reached saturation, the resonant wavelength increased no longer and maintained a certain value. As shown in Fig. 4a, when the concentrations of rabbit anti-goat IgM are 50, 75, 100 and 125 μg mL^{-1}, the shifts of resonant wavelength are 5.10, 5.77, 6.88 and 6.96 nm, respectively. As a result, 100 μg mL^{-1} was chosen as the optimal concentration of rabbit anti-goat IgM for the detection of goat IgM.

In order to study the effects of Fe_3O_4–AuNR nanocomposites on performance improvement for the SPR biosensor, the biosensor based on MPA/anti-goat IgM sensing membrane was also investigated. 100 μg mL^{-1} rabbit anti-goat IgM was used to prepare the MPA/anti-goat IgM sensing membrane. Fig. 4b shows the kinetic adsorption curves of anti-goat IgM immobilized on Fe_3O_4–AuNR nanocomposites sensing membrane and MPA sensing membrane. Obviously, the amount of rabbit anti-goat IgM immobilized on Fe_3O_4–AuNR nanocomposites is larger than that immobilized on MPA.

3.4. Determination of goat IgM

At room temperature, after the rabbit anti-goat IgM was immobilized on the surface of the biosensor, goat IgM was injected into the flow cell. The shifts of resonant wavelength caused by antibody–antigen immunoreaction were monitored in real time. Fig. 5 draws the relationship between the concentrations of goat IgM and the shifts of resonant wavelength obtained with the biosensors based on Fe_3O_4–AuNR nanocomposites

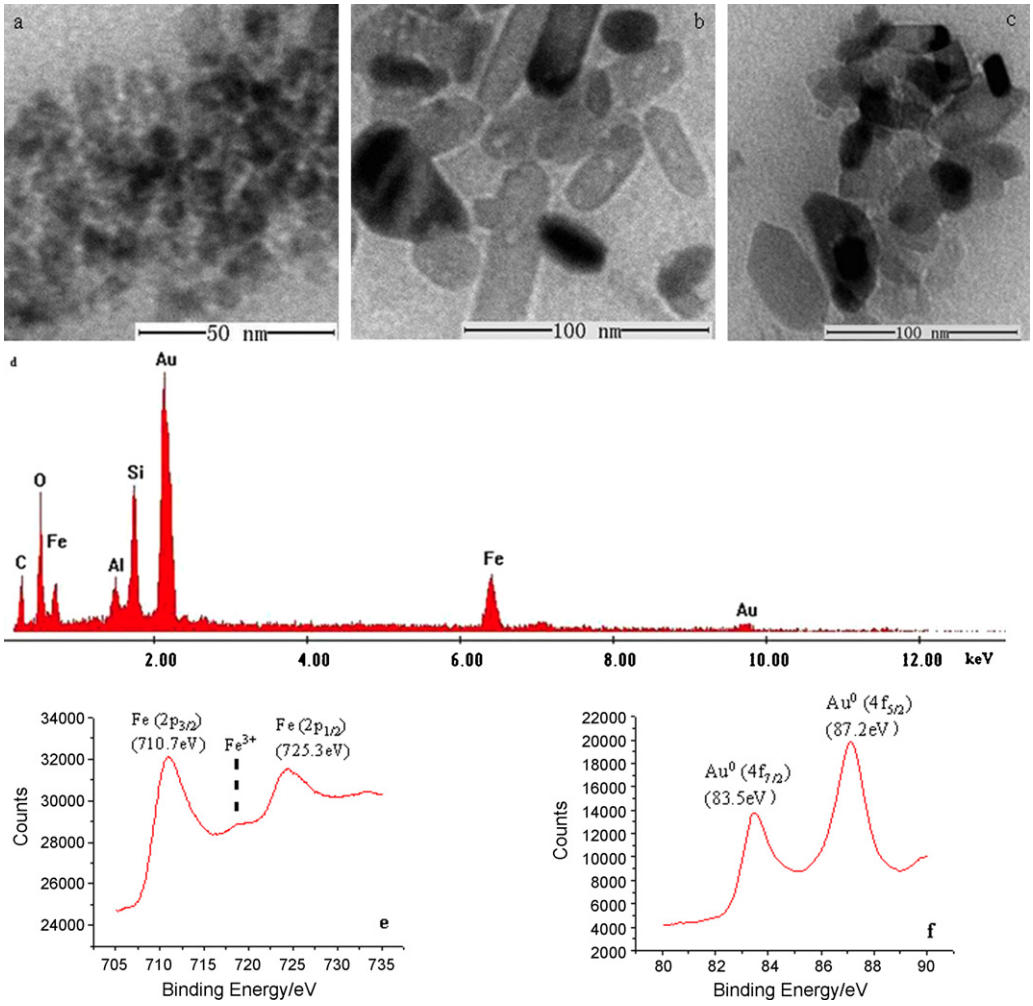

Fig. 2. TEM images of Fe_3O_4 nanoparticles (a), Fe_3O_4–AuNR nanocomposites (b and c), energy dispersive spectrum of Fe_3O_4–AuNR nanocomposites (d) and X-ray photoelectron spectra of Fe (e) and Au (f).

and MPA membrane. It can be seen from Fig. 5a that the SPR biosensor based on Fe_3O_4–AuNR/anti-goat IgM sensing membrane shows a good response to goat IgM in the concentration range of 0.15–40.00 μg mL^{-1}. The minimum shift of resonant wavelength is 0.44 nm at 0.15 μg mL^{-1} and the maximum shift of resonant wavelength is 5.54 nm at 40.00 μg mL^{-1}. The SPR biosensor based on MPA/anti-goat IgM sensing membrane shows a good response to goat IgM in the concentration range of 1.25–40.00 μg mL^{-1}. The minimum shift of resonant wavelength is 0.44 nm at 1.25 μg mL^{-1} and the maximum shift of resonant wavelength is 2.66 nm at 40.00 μg mL^{-1}. As mentioned above, the experimental results indicated that the application of Fe_3O_4–AuNR nanocomposites highly improved the performance of the wavelength-modulation SPR biosensor. The limit of quantification (LOQ) is defined as the lowest concentration of an analyte that can be quantitatively determined by the proposed method. Under identical conditions, the LOQ obtained from the biosensor modified with Fe_3O_4–AuNR nanocomposites is

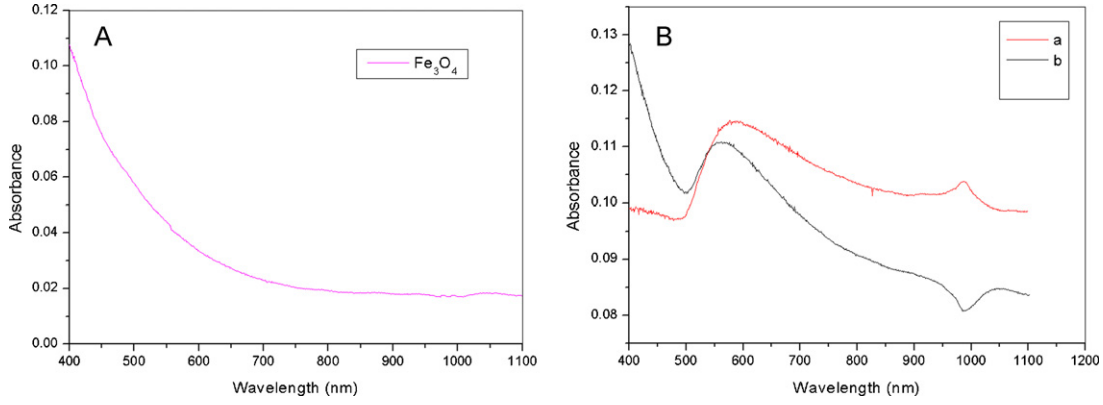

Fig. 3. UV–vis–NIR absorption spectra of Fe_3O_4 nanoparticles (A) and Fe_3O_4–AuNRs nanocomposites (B).

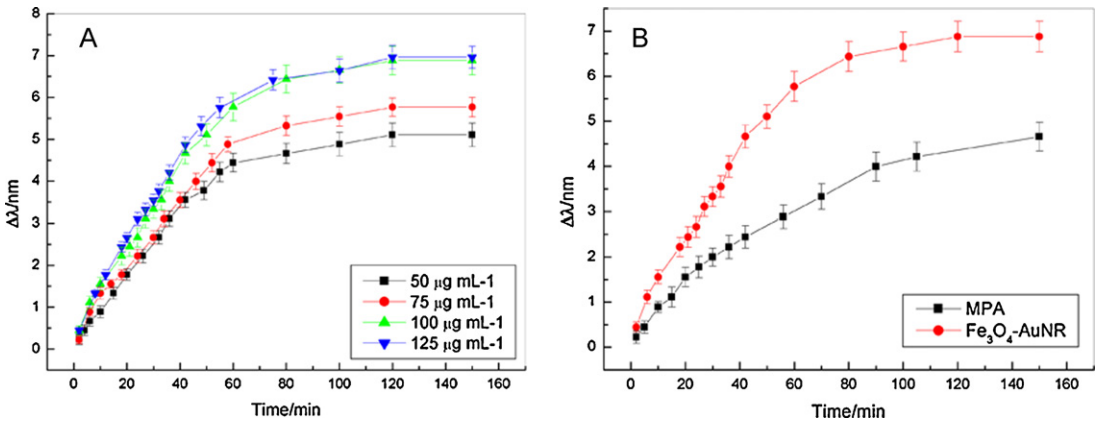

Fig. 4. (a) The kinetic adsorption curves of immobilizing rabbit anti-goat IgM (b) The kinetic adsorption curves of rabbit anti-goat IgM at the concentration of 100 μg mL^{-1}.

eight-fold lower than that obtained with MPA membrane biosensor.

When Au nanorod is combined with Fe_3O_4 nanoparticles, the resulting nanocomposites exhibit exceptional optical property as well as magnetic property. Au nanorod has its own localized surface plasmon due to the collective oscillation of its conduction electrons, leading to a strong local electromagnetic field near Fe_3O_4–AuNR nanocomposites. The interaction between the localized surface plasmon of Au nanorod and the propagating plasmon in the Au film gave rise to the shift of resonant wavelength of SPR biosensor. On the other hand, as the Fe_3O_4–AuNR nanocomposites were immobilized on the surface of biosensor chip, the thickness of the sensing membrane increases and the resonant wavelength produces red shifts, which results in the sensitivity enhancement of the wavelength-modulation SPR biosensor.

The reaction between antigen (Ag) and antibody (Ab) can be expressed as follows: Ag + Ab = AgAb, the binding constant is K_A:

$$K_A = \frac{[AgAb]}{[Ag][Ab]} \quad (1)$$

where [AgAb] is the concentration of AgAb on the sensor surface, which corresponds to the SPR biosensor signal at equilibrium $\Delta\lambda_{eq}$, [Ag] is the concentration of antigen in the solution, [Ab] is the concentration of Ab on the sensor surface, which corresponds to $(\Delta\lambda_{max} - \Delta\lambda_{eq})$. $\Delta\lambda_{max}$ is the SPR response corresponding to the maximum capacity of binding antigen on the sensor surface. So Eq. (1) can be expressed as:

$$\frac{\Delta\lambda_{eq}}{Ag} = K_A\Delta\lambda_{max} - K_A\lambda_{eq} \quad (2)$$

$\Delta\lambda_{eq}$ increases with the increase of [Ag] in the solution. However, it can be seen from Eq. (2) that $\Delta\lambda_{eq}$/[Ag] decreases with the increase of $\Delta\lambda_{eq}$. So the slope of the relationship curve between the shift of the resonant wavelength and the concentration of Ag decreases with the increase of the concentration of Ag, which is in accordance with the experimental result. Because the response is not linear, the sensitivity was not expressed by the slope of the calibration curve and the performance was described by LOQ.

The specificity is also demonstrated by detecting human IgG and BSA under the same conditions. After the rabbit anti-goat IgM was immobilized on the biosensor surface chip, human IgG and BSA at the concentration of 10 μg mL^{-1} were separately injected into the flow cell for 30 min. There were no observable shifts in the resonant wavelength (Fig. 6), which indicated the selective binding of goat IgM.

3.5. Regeneration of biosensor

After the magnetic pillar was taken away from under the prism, the Fe_3O_4–AuNR nanocomposites coupled with anti-goat IgM could be dissociated from the biosensor chip surface by injecting water

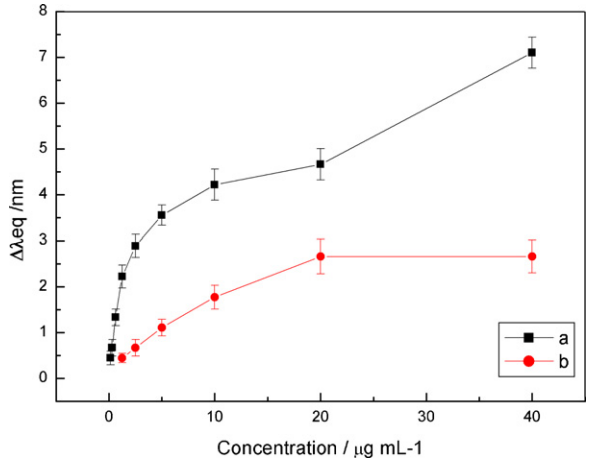

Fig. 5. The relationship between the concentrations of goat IgM and the shifts of resonant wavelength obtained with the biosensor based on Fe_3O_4–AuNR nanocomposites (a) and MPA (b).

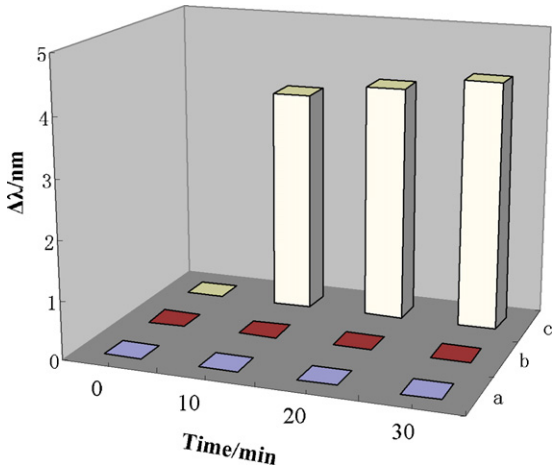

Fig. 6. Kinetic response of human IgG (a), BSA (b) and goat IgM (c) detected by SPR biosensor based on Fe_3O_4–AuNR nanocomposites.

into the flow cell. The SPR response curve of the whole cycle includes the immobilization of Fe_3O_4–AuNR nanocomposites and antibody, the binding of antigen and antibody and the regeneration of the biosensor (Fig. S4).

4. Conclusions

A wavelength modulation SPR biosensor based on Fe_3O_4–AuNR nanocomposites was constructed and applied to the detection of goat IgM. Fe_3O_4–AuNR nanocomposites were proved to be ideal carriers to bind proteins due to their good biocompatible and exceptional optical properties. Au nanorods show two kinds of plasmon absorption bands, especially the longitudinal plasmon band which is more sensitive to the changes in the dielectric properties of the surroundings. AuNR coupled with magnetic Fe_3O_4 nanoparticles can be easily immobilized on the biosensor chip surface with a magnetic pillar, which simplifies the experimental procedure. The experimental results indicate that the biosensor based on Fe_3O_4–AuNR nanocomposites exhibits a satisfactory response to goat IgM in the concentration range of 0.15–40.00 $\mu g\,mL^{-1}$. Therefore, the Fe_3O_4–AuNR nanocomposites play a crucial role in performance improvement of SPR biosensor.

Acknowledgements

This work was supported by National Natural Science Foundation of China (Nos. 20727003, 21075049, 21105037), Program for New Century Excellent Talents in University (No. NECT-10-0443) and Science and Technology Developing Foundation of Jilin Province (Nos. 20100356, 20110162).

Appendix A. Supplementary data

Supplementary data associated with this article can be found, in the online version, at doi:10.1016/j.bios.2012.01.032.

References

Barr, T.L., 1978. J. Phys. Chem. 82, 1801–1810.
Caiazzo, M., Alessandrini, A., Facci, P., 2009. Appl. Mater. Interfaces 1, 514–525.
Chen, H.J., Kou, X.S., Yang, Z., 2008. Langmuir 24 (10), 5233–5237.
Chou, S.F., Hsu, W.L., Hwang, J.M., Chen, C.Y., 2004. Biosens. Bioelectron. 19, 999–1005.
Danelian, E., Karlén, A., Karlsson, R., Winiwarter, S., Hansson, A., öfås, L., Lennernäs, S., Hämäläinen, H.M.D., 2000. J. Med. Chem. 43, 2083–2086.
Daniel, M.C., Astruc, D., 2004. Chem. Rev. 104, 293–346.
Eum, N.S., Yeom, S.H., Kwon, D.H., Kim, H.R., Kang, S.W., 2010. Sens. Actuators B 143, 784–788.
Fujino, T., Sato, Y., Une, M., Kanayasu-Toyoda, T., Yamaguchi, T., Shudo, K., Inoue, K., Nishimaki-Mogami, T., Steroid, J., 2003. Biochem. Mol. Biol. 87, 247–252.
Härtling, T., Uhlig, T., Seidenstücker, A., Bigall, N.C., Olk, P., 2010. Appl. Phys. Lett. 96, 183111.
He, L., Smith, E.A., Natan, M.J., Keating, C.D., 2004. J. Phys. Chem. B 108, 10973–10980.
Hegde, V., Wang, M., Deutsch, W.A., 2004. DNA Repair 3, 121–126.
Hu, S.H., Tsai, C.H., Liao, C.F., Liu, D.M., Chen, S.Y., 2008. Langmuir 24, 11811–11818.
Ito, A., Shinkai, M., Honda, H., Kobayashi, T., 2005. J. Biosci. Bioeng. 100, 1–11.
Jain, P.K., Eustis, S., El-Sayed, M.A., 2006. J. Phys. Chem. B 110, 18243–18253.
Jana, N.R., Gearheart, L., Murphy, C., 2001. J. Adv. Mater. 13, 1389–1393.
Kouassi, G.K., Irudayaraj, J., 2006. Anal. Chem. 78, 3234–3241.
Law, W.C., Yong, K.T., Baev, A., Prasad, N.P.N., 2011. ACS Nano 5, 4858–4864.
Lee, K.S., El-Sayed, M.A., 2006. J. Phys. Chem. B 110, 19220–19225.
Link, S., El-Sayed, M.A., 2005. J. Phys. Chem. B 109, 10531–10532.
Liu, W., Zhang, Z.D., Liu, J.P., Chen, L.J., He, L.L., Liu, Y., Sun, X.K., Sellmyer, D.J., 2002. Adv. Mater. 24, 1832–1834.
Liu, H.Y., Chen, D., Yang, L.Q., Ren, X.L., Tang, F.Q., Ren, J., 2010. Nanotechnology 21, 185504.
Malik, M.A., O'Brien, P., Revaprasadu, N., 2002. Chem. Mater. 14, 2004–2010.
Negishi, Y., Nobusada, K., Tsukuda, Y., 2005. J. Am. Chem. Soc. 127, 5261–5270.
Nikoobakht, B., El-Sayed, M.A., 2003. Chem. Mater. 15 (10), 1957–1962.
Pérez, N.P., Gao, Y., Hilgendorff, M., Irsen, S., Juste, J.P., Spasova, M., Farle, M., Marzán, L.M.L., Giersig, M., 2007. Chem. Mater. 19, 4415–4422.
Peña, O., Pal, U., Fernández, L.R., Silva-Pereyra, H.G., Iglesias, V.R., Wong, J.C.C., Alatorre, J.A., Oliver, A., 2009. J. Phys. Chem. C 113, 2296–2300.
Rich, R.L., Day, Y.S.N., Morton, T.A., Myszka, D.G., 2001. Anal. Biochem. 296, 197–207.
Salem, A.K., Searson, P.C., Leong, K.W., 2003. Nat. Mater. 2, 668.
Sun, Y., Bai, Y.P., Song, D.Q., Li, X.Z., Wang, L.Y., Zhang, H.Q., 2007. Biosens. Bioelectron. 23, 473–478.
Wang, C.T., Ro, S.H., 2006. J. Non-Cryst. Solids 352, 35–43.
Wang, C.G., Ma, Z.F., Wang, T.T., Su, Z.M., 2006. Adv. Funct. Mater. 16, 1673–1678.
Wang, L.Y., Sun, Y., Wang, J., Zhu, X.N., Jia, F., Cao, Y.B., Wang, X.H., Zhang, H.Q., Song, D.Q., 2009. Talanta 78, 265–269.
Wang, J., Song, D.Q., Wang, L.Y., Zhang, H., Zhang, H.Q., Sun, Y., 2011. Sens. Actuators B 157, 547–553.
Weizmann, Y., Patolsky, F., Katz, E., Willner, I., 2003. J. Am. Chem. Soc. 125, 3452–3454.
Yu, H., Chen, M., Rice, P.M., Wang, S.X., White, R.L., Sun, S.H., 2005. Nano Lett. 5, 379–382.
Zeng, H., Li, J., Liu, J.P., Wang, Z.L., Sun, S.H., 2002. Nature 420, 395–398.
Zhao, X.L., Cai, Y.Q., Wang, T., Shi, Y.L., Jiang, G.B., 2008. Anal. Chem. 80, 9091–9096.